This is the Pre-Published Version.

C. Fan, D. Luan, R. Bu, Z. Sheng, F. Wang, X. Huang (2023) *Can heavy rainfall affect the burning and smoke spreading characteristics of fire in tunnels?* **International Journal of Heat and Mass Transfer**, 207, 123972. https://doi.org/10.1016/j.ijheatmasstransfer.2023.123972

Can heavy rainfall affect the burning and smoke spreading characteristics of fire in tunnels?

Chuangang Fan[1], Dia Luan[1], Rongwei Bu[1], Ziqiong Sheng[1], Feiyue Wang[1,*], Xinyan Huang[2,*]

[1]*School of Civil Engineering, Central South University, Changsha, China*

[2]*Department of Building Environment and Energy Engineering, The Hong Kong Polytechnic University, Kowloon, Hong Kong, China*

*Corresponding Authors: wfycsu@csu.edu.cn (F. Wang); xy.huang@polyu.edu.hk (X. Huang)

Abstract

Extreme rainfall events are increasingly common under the current trend of global warming. This work investigates how heavy rainfall on one exit affects the fire burning and the smoke spread in tunnels. Several reduced-scale tests are designed with various rainfall intensities (up to 60 mm/h, equivalent to 232 mm/h in nature), raindrop sizes (1.0-1.5 mm, equivalent to 4-6 mm in nature), and tunnel fire heat release rates (2.1-6.7 kW, equivalent to 2-6 MW in real scale). Experiments show that heavy rainfall on one exit can induce a longitudinal airflow inside the tunnel, and the induced airflow is caused by an increase in pressure of the rainfall exit. The airflow pushes the flame tilting towards the no-rainfall portal, and the correlation among the flame length and flame inclination, the induced airflow and rainfall is explained by an analytical model. The rainfall-induced airflow has a limited effect on the burning rate of pool fires, but it can change the ceiling temperature and limit the smoke back-layering toward the rainfall portal. In contrast, the ceiling temperature distribution towards the no-rainfall portal is not sensitive to rainfall, which can be well described by an empirical model.

Keywords: *Tunnel fire; Rainfall effect; Flame length; Burning rate; Ceiling temperature; Smoke back-layering*

Nomenclature

Symbols		S	cross-section area of the raindrop (m^2)
A	pool area (cm^2)	V	volume (m^3)
C_D	drag coefficient (-)	V_d	volume of a single raindrop (m^3)
d_0	median volume drops diameter (mm)	v	velocity (m/s)
d_f	diameter of the fire source (m)	v_T	terminal velocity of raindrop (m/s)
E	energy (kJ)	$v_{a,0}$	airflow velocity at tunnel portal (m/s)
Fr	Froude number (-)	v_p	velocity by rain-induced pressure (m/s)
G	acceleration of gravity (m/s^2)	x	distance from the fire source (m)
H	tunnel height (m)	X_f	Horizon ,tal flame length (cm)
h_f	flame height (cm)	**Greek Symbols**	
I	rainfall intensity (mm/h)	ρ	density (kg/m^3)
I^*	dimensionless rainfall intensity (-)	θ	flame inclination (°)
L	tunnel length (m)	φ	volume ratio of all raindrops (-)
L_f	total flame length (cm)	Δ	difference between variables
$\dot{m}$	mass flow rate (kg/s)	**Subscripts**	
$\dot{m}''$	mass burning rate per area (g/m^2-s)	a	ambient condition
$\dot{m}'''$	mass flux of raindrops (kg/m^2-s)	w	water
$\dot{N}''$	number flux of raindrops (#/m^2-s)	max	maximum
P	ambient pressure (kPa)	F	full tunnel
Q	heat release rate (kW)	M	model tunnel

1. Introduction

Centuries of global industrialization have raised the concentration of greenhouse gases in the atmosphere and the problem of global warming. Today, human beings are facing more climate change problems, like El Niño, extreme weather, and more frequent massive wildfires, which will occur more frequently in recent decades [1,2]. Recently, both the intensity and frequency of rainfall have been increasing, potentially due to climate change [3]. Especially, the heat island effects and the increased roughness of urban surfaces can increase rainfall intensity in urban areas [4].

The increasing number of urban tunnels and vehicles implies an increase in the risk of tunnel fires in terms of fire suppression, smoke extraction, evacuation and rescue. In view of its major importance as a part of the urban infrastructure, the fire safety of tunnels warrants a great deal of attention. According to the survey [5,6], the accident rate in the entrance zone of the tunnel is higher than in other zones, and rainfall exacerbates the risk of tunnel fires due to increased accidents. In particular, the extreme rainfall event that occurred in Zhengzhou, China, in 2021 [7] has aroused concerns about tunnel fire accidents under heavy rainfall conditions. Therefore, we will expect more tunnel fire incidences under more frequent extreme weather and rain events.

For a fire inside the confined tunnel space, the inherent properties of the tunnel, such as geometry, tunnel slope, tunnel length, and tunnel ramp, have a significant impact on burning and smoke spreading characteristics in tunnel fires [8, 9]. The spread of smoke in the opposite direction to ventilation is called “back-layering”, and the back-layering length is defined as the length of the reverse smoke flow [10]. Zhang et al. [11] studied the back-layering length in a longitudinally ventilated tunnel with various rectangular cross-sections, and the prediction correlations of back-layering length were proposed considering the aspect ratio. Ji et al. [12] studied the smoke behavior in inclined road tunnels by numerical simulation. It was found that the upstream smoke layer interface was parallel to the horizontal level while the downstream smoke layer interface was parallel to the inclined tunnel ceiling. Shafee and Yozgatligil [13] analyzed the effects of vehicular blockage and tunnel inclination and showed that the burning rate and ceiling temperature increased when a blockage was present, and the heat release rate (HRR) of fire increased in downhill-inclined cases. Ishikawa et al. [14] found that in the case of a long tunnel, descending smoke and backflow of air vitiated occurs, and for a vitiated fire, the chemical HRR of the fire decreases to half or less than that of the normal fire. Huang et al. [15] studied the thermal smoke movement behavior of the branched tunnel under the synergistic effects of bifurcation angle and longitudinal ventilation velocity by carrying out several reduced-scale experiments, and an empirical model of back-layering length was proposed.

As the burning body of the tunnel fire event, the type of fuel, the amount of fuel, and the location of the fire source all play an important role in burning and smoke spread. Jia et al. [16] investigated the ceiling temperature profile induced by double pool fires in a tunnel. Results showed that the ceiling temperature distribution still conformed to the exponential decay law for double fires in a tunnel, and a correction for predicting the ceiling temperature decay was proposed by introducing fire size and fire spacing. Gannouni [17] studied the critical velocity

and smoke temperature for a fire developing in different locations relative to the tunnel floor. The results showed the critical velocity decreases and the maximum smoke flow temperature increases with the increases of the fire location from the tunnel floor. Fan et al. [18] conducted a series of scale tests to investigate the influence of sidewall on flame characteristics of heptane pool fires in a channel, and the distance between fire and sidewall was changed. They found the sidewall had a restriction effect on the air entrainment of the fire plume and developed an integral flame length model considering both the sidewall effect and fuel shape.

In addition, the external environment, including ambient pressure, oxygen concentration, external wind, etc., also affects the tunnel fire characteristics. Tang et al. [19] examined the impact of pressure on the longitudinal distribution of smoke temperature and found that the longitudinal decay of the smoke flow temperature along the tunnel was faster in the reduced-pressure atmosphere. Yan et al. [20] tested six fires inside a road tunnel located 4100 m above sea level to examine the heat release rates (HRR), temperature distributions, and smoke spreading. Results showed that compared with normal altitude fires, the high-altitude fire has a lower mass loss rate and a slower decay in the dimensionless temperature. Wu et al. [21] investigated how atmospheric pressure affected smoke back-layering during a subway tunnel fire by numerical simulation and found that the length of smoke back-layering increased as decreasing atmospheric pressure for a given HRR and ventilation velocity.

Yao et al. [22] investigated the fire characteristics with inadequate ventilation in model-scale and medium-scale tunnels and found that under-ventilation fire showed a reduction in mass loss per unit area and flame size. Lin et al. [23] experimentally analyzed the self-extinction behaviors in a reduced-scale tunnel with different boundary materials and found that the longitudinal temperature attenuation was dominated by the markup flow. Salizzoni et al. [24] studied experimentally the extent of the back-layering flow developing below the ceiling of a longitudinally ventilated tunnel. It was found that the heat loss at the tunnel walls was nonnegligible for the back-layering flow. Zhong et al. [25] studied the bifurcation flow of smoke in the tunnel with longitudinal ventilation by numerical simulation, and the generation mechanism of smoke bifurcation flow was revealed. Tanaka et al. [26] conducted several fire experiments inside a shallow urban road tunnel equipped with roof openings to investigate the flow structure under the external longitudinal wind, and a prediction model of smoke-spreading length was proposed. Yi et al. [27] conducted several model tests to investigate the effect of the canyon crosswind on the flow field and the tunnel fire behavior. They showed that an uneven flow field was formed inside the tunnel under the effect of the canyon crosswind, and the fire behavior varied with fire locations.

In our previous work [28], the impact of heavy rainfall on the smoke movement and stratification dynamics in tunnel fires have been investigated. Would the fire burning and smoke spreading characteristics be different in tunnel fires under the effect of extreme rainfall? This is the motivation for this study. To this end, a series of model-scale tests were conducted in this paper. The project will provide a completely new perspective on how heavy rainfall affects tunnel fires and provide guidance for rapid rescue in emergencies.

2. Experimental details

2.1 Rainfall simulator

At present, artificial rainfall simulation technology is quite mature and widely used in surface hydrology and soil science research. The nozzles generating rainfall were divided into five groups and installed 3.53 m above the simulated ground. Set the desired rainfall intensity and select nozzles to be activated in the central controller user interface. Real-time rainfall intensity was obtained by a rain gauge with an accuracy of 0.1 mm and fed back to the central controller synchronously. The central controller adjusted the real-time rainfall intensity to the set value by controlling the pump pressure, and the error was less than 5%.

The China Meteorological Administration [29] defines a rainfall intensity that exceeds 50 mm within 24 hours is considered as heavy rainfall. However, extreme rainfall events have frequently occurred in recent years, and the rainfall intensity may reach a very high value during a certain period of time. For example, the maximum hourly rainfall of the extreme rainfall event reached 184.4 mm during 6-7 May 2017, which occurred in Guangzhou, China [30]. Maximum hourly rainfall of 201.9 mm was also recorded during 17-23 July 2021 in Zhengzhou, China [7]. It can be seen that the instantaneous rainfall intensity has far exceeded 50 mm within 24 hours. Therefore, the instantaneous rainfall intensity was the concern in the study.

Raindrops in nature usually have a diameter between 0.5 mm and 6.0 mm, which tends to increase with rainfall intensity [31]. Many factors affect the raindrop size distribution according to previous research, such as climate, location, season, and so on [32]. Therefore, in the experiment, three raindrop diameters were used to investigate the effect of raindrop size with the same rainfall intensity.

2.2 Experimental setup

In this study, the Froude similarity criterion was employed as the scale basis [33], and the important scale correlations are listed in Table 1. A reduced-scale experimental platform with a scale of 1:15 was designed based on the correlations, which included a tunnel model and an

artificial rainfall simulator in Fig. 1. The tunnel model was 10 m long, 0.6 m wide, and 0.4 m high, consisting of 5 tunnel model units with a length of 2 m. The top, bottom, and one sidewall of the tunnel model were made of calcium silicate plates of 20 mm thickness. The fireproof glass of 8 mm thickness was arranged on the other sidewall to observe and record the experimental process. The rainfall was generated by the artificial rainfall simulator. Asymmetric rainfall was considered in this work, where the rainfall simulator was only set on one exit of the tunnel. The effective rainfall area was 2.0 m × 2.0 m, which could cover the tunnel portal completely. The uniformity estimated by the Christiansen coefficient was greater than 88%.

Table 1. Scaling correlations of some key parameters.

Parameters	Symbol	Scaling correlation
Length	L (m)	L_M/L_F =1:15
Heat release rate	Q (kW)	$Q_M/Q_F=(L_M/L_F)^{5/2}$
Mass flow rate	$\dot{m}$ (kg/s)	$\dot{m}_M/\dot{m}_F=(L_M/L_F)^{5/2}$
Velocity	v (m/s)	$v_M/v_F=(L_M/L_F)^{1/2}$
Energy	E (kJ)	$E_M/E_F=(L_M/L_F)^{3}$
Rainfall intensity	I (mm/h)	$I_M/I_F=(L_M/L_F)^{1/2}$
Raindrop diameter	d_0 (mm)	$d_{0,M}/d_{0,F}=(L_M/L_F)^{1/2}$
Temperature	T (K)	$T_M=T_F$

The subscripts M and F represent model-scale and full-scale, respectively.

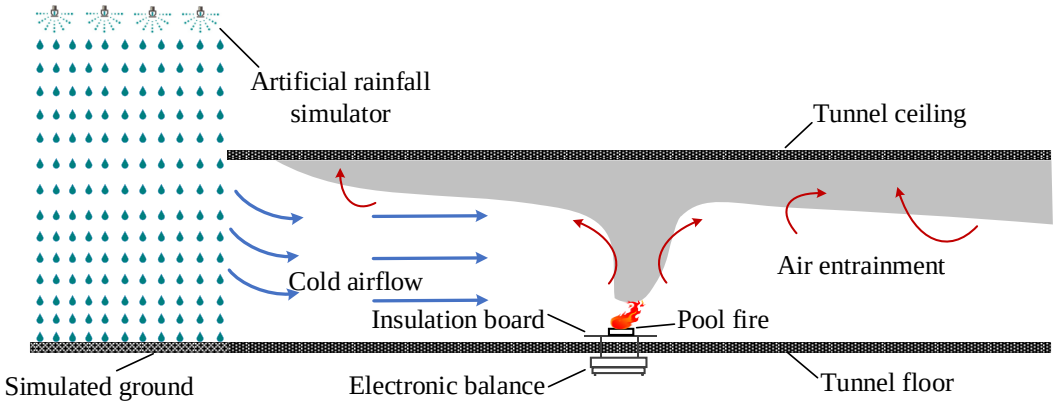

Fig. 1 Schematic diagram of the experimental platform.

As a fuel source, absolute ethanol was chosen because its safety and cleanliness make it suitable for laboratory use. The physical properties of the fuel are provided in Table 2. Three square fuel pools with different HRRs were located at the center of the tunnel, and the upper edge of the fuel pool was 3 cm from the tunnel floor. The initial fuel depth was fixed as 8 mm for all cases. The mass loss history of the fuel was measured by an electronic balance with an

accuracy of 0.1 g and then transmitted to a computer at a frequency of 1 Hz for recording. Thus, both the burning rate and HRR in the steady state could be obtained. A total of 51 K-type thermocouples were uniformly arranged 2 cm beneath the ceiling with a longitudinal interval of 0.2 m to measure the ceiling temperature distribution. In a digital video recording with 50 frames per second, flame morphology development was observed. Table 3 details the experimental conditions, and a total of 48 tests were performed. Each group was repeated twice to ensure good repeatability.

Table 2. Properties parameters of the fuel.

Material	Concentration (%)	Density (kg/m^3)	Heat of combustion (kJ/g)	Combustion efficiency (-)
Ethanol	99.7	0.79	26.8	0.994

Table 3. Experimental conditions, where HRR shown is a baseline value without rainfall.

Case No.	*Rainfall intensity Test [Nature]* I (mm/h)	*Raindrop size* d_0 (mm)	*Pool area* A (cm^2)	*Fire HRR Test [Real-scale]* (kW) [MW]
1-3	0 [0]	1.0, 1.2, 1.5	64	2.1 [1.8]
4-12	20 [77]			
13-21	30 [116]		100	4.3 [3.8]
22-30	40 [155]		144	6.7 [5.9]
31-39	50 [194]			
40-48	60 [232]			

3. Results and discussion

3.1 Rain-induced wind effect

Figure 2 shows the velocity distribution of the induced longitudinal airflow in the tunnel under various rainfall intensities and raindrop sizes, which is measured by a hand-held hot-wire anemometer with an accuracy of 0.01 m/s. The velocity probes of hot wire have been used for flow characterization in various flow conditions [34]. The velocities of the upper, middle, and lower points of the same tunnel section were measured, showing good airflow uniformity. Therefore, the velocity of the center point of the tunnel section was used to replace the average velocity of the entire section. The measuring locations were set at the center of each tunnel unit, and the section velocity of the portal with rainfall was also measured. The airflow velocity inside the tunnel was measured repeatedly to ensure reliability. It is evident that the airflow

velocity increases with the increasing rainfall intensity. The smaller raindrop size means a larger induced airflow velocity for a given rainfall intensity, and the influence of raindrop size on the induced airflow velocity decreases with increasing rainfall intensity.

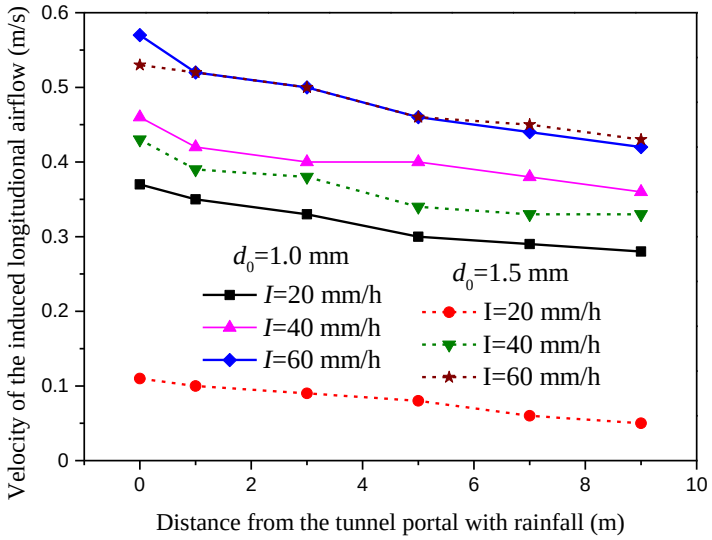

Fig. 2 Velocity distribution of the induced longitudinal airflow with different I and d_0.

With the continuous falling of raindrops, the local ambient pressure is increased at the tunnel portal with the rainfall, so an expansion airflow is induced. At the tunnel portal, a longitudinal airflow is induced in the tunnel due to the dissipation of dynamic pressure. Thus, the velocity of the induced longitudinal airflow at the tunnel portal with rainfall ($v_{a,0}$) should be correlated to the characteristic velocity (v_p) caused by the rainfall-induced dynamic pressure.

Here, we make two key assumptions, (1) the increase of ambient pressure is caused by the volume increase of all raindrops, and (2) the raindrop is a sphere. The terminal velocity of the spherical raindrop can be calculated by the balance between gravity ($m_d g$) and the air drag [35], as

$$m_d g \approx \frac{1}{2} C_D \rho_a v_T^2 S \tag{1}$$

Then, the terminal velocity of the raindrops can be estimated by

$$v_T = \sqrt{\frac{2 m_d g}{C_D \rho_a S}} = \sqrt{\frac{\rho_w d_0 g}{\left(\frac{3}{4}\right) C_D \rho_a}} \tag{2}$$

where the raindrop mass is $m_d = \rho_w \frac{\pi}{6} d_0^3$, the raindrop cross-section is $S = \frac{\pi}{4} d_0^2$, and for simplicity, C_D =0.47 is chosen for a sphere [36]. Table 4 summarizes the characteristic parameters of tested raindrops with three different diameters.

Table 4. Basic information of tested three raindrops.

Raindrop Parameter	Expression	Value		
Diameter of raindrop	d_0 (mm)	1.0	1.2	1.5
Cross-section area	$S = \frac{\pi}{4} d_0^2$ (m^2)	7.854×10^{-7}	1.131×10^{-6}	1.767×10^{-6}
Volume of a raindrop	$V_d = \frac{\pi}{6} d_0^3$ (m^3)	0.52×10^{-9}	0.90×10^{-9}	1.77×10^{-9}
Mass of a raindrop	$m_d = \rho_w \frac{\pi}{6} d_0^3$ (kg)	0.52×10^{-6}	0.90×10^{-6}	1.77×10^{-6}
Terminal velocity	$v_T = \sqrt{\frac{\rho_w d_0 g}{\left(\frac{3}{4}\right) C_D \rho_a}}$ (m/s)	4.64	5.09	5.69

The rainfall intensity (I) determines the number of raindrops per unit area per unit of time ($\dot{N}''$ or the raindrop flux) as

$$\dot{N}'' = \frac{I\rho_w}{m_d} = \frac{I}{V_d} \tag{3}$$

where $V_d = \frac{\pi}{6} d_0^3$ is the volume of a single raindrop. The volume ratio of all raindrops in the ambient can be calculated by

$$\varphi = \frac{\Delta V}{V} = \frac{\dot{N}'' V_d}{v_T} \tag{4}$$

Then, the pressure increased by these additional raindrops can be calculated by

$$\Delta P = P_a \varphi \tag{5}$$

Therefore, the velocity (v_p) caused by the increased dynamic pressure at the rainfall exit can be expressed as

$$v_p = \sqrt{\frac{2\Delta P}{\rho_a}} = \sqrt{\frac{2P_a}{\rho_a}\frac{\dot{N}'' V_d}{v_T}} = \sqrt{\frac{2P_a}{\rho_a}\frac{I}{\sqrt{\frac{\rho_w d_0 g}{0.75 C_D \rho_a}}}} = \sqrt{2P_a I \sqrt{\frac{0.75 C_D}{\rho_a \rho_w d_0 g}}} \propto I^{\frac{1}{2}} d_0^{-\frac{1}{4}} \tag{6}$$

which increases with the rainfall intensity (I) while decreases with the raindrop diameter (d_0). Table 5 lists the correlation between raindrops and rainfall and the rainfall-induced pressure

and flow changes under the rainfall intensity of I = 20 mm/h.

Table 5. Rainfall characteristics and environmental changes under I=20 mm/h.

Rainfall Parameter	Expression	Values (under I=20 mm/h) d_0=1.0 mm	d_0=1.2 mm	d_0= 1.5 mm
Mass flux of rain fall	$\dot{m}''' = I\rho_w = m_d\dot{N}''$ (kg/m^2-s)	0.0056	0.0056	0.0056
Number flux of raindrops	$\dot{N}'' = \frac{I\rho_w}{m_d} = \frac{I}{V_d}$ (#/m^2-s)	10616	6143	3145
Volume ratio of all raindrops	$\varphi = \frac{\Delta V}{V} = \frac{\dot{N}''V_d}{v_T}$ (-)	1.20×10^{-6}	1.09×10^{-6}	9.77×10^{-7}
Pressure increase	$\Delta P = P_a\varphi$ (Pa)	0.120	0.109	0.098
Pressure-induced velocity	$v_p = \sqrt{\frac{2\Delta P}{\rho_a}}$ (m/s)	0.43	0.41	0.39

Figure 3 shows the relationship between $v_{a,0}$ and v_P, where $v_{a,0}$=$0.7v_P$ can give an excellent linear fit with R^2 coefficient of 0.96. Then, the velocity of the induced longitudinal airflow where the tunnel portal with rainfall can be expressed as

$$v_{a,0} = 0.7v_p = 0.8\left(P_a I\right)^{\frac{1}{2}}\left(\rho_a\rho_w d_0 g\right)^{-\frac{1}{4}} \propto I^{\frac{1}{2}}d_0^{-\frac{1}{4}} \tag{7}$$

which also increases with the rainfall intensity (I) while decreasing as the raindrop diameter increases (d_0).

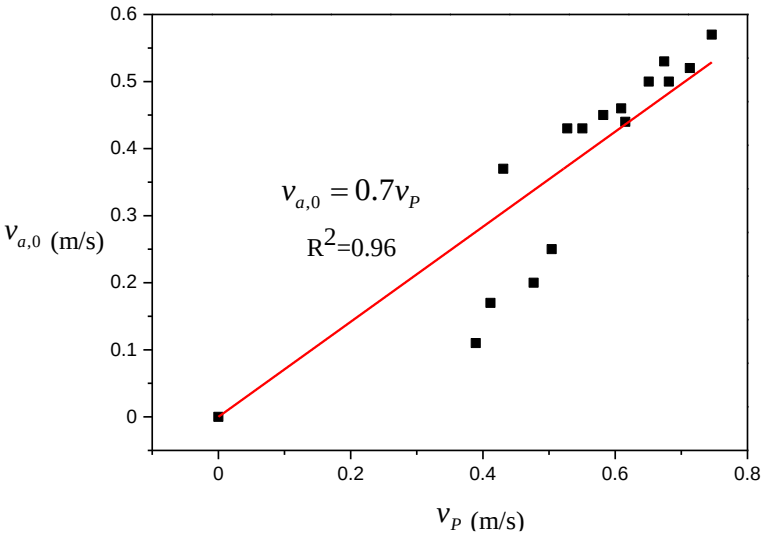

Fig. 3 Relationship between $v_{a,0}$ and v_p.

On the other hand, the velocity of the induced airflow in the tunnel decreases along the length direction owing to viscous drag in fluids, as shown in Fig. 2. It is conceivable that if the tunnel is long enough, the airflow velocity in the tunnel will eventually decay to 0. However, due to the short tunnel length, the outlet airflow velocity is not zero. However, it can still provide new insight into the understanding of tunnel fire characteristics under heavy rainfall conditions, especially the fire occurring near the tunnel portal.

3.2 Combustion characteristic

Characterizing the combustion of pool fires requires understanding flame behavior and burning rate [37]. On the one hand, the longitudinal airflow induced by rainfall tilts the flame, which is likely to ignite the downstream combustibles and expand the fire area [38]. On the other hand, the tilted flame could alter the thermal feedback mechanism of pool fire, which may lead to faster burning and greater HRR [39].

It is noted that the HRR values in the following discussion are characterized by the measured value without rainfall. Figure 4 shows the flame shape under different rainfall intensities and raindrop sizes with HRR=2.1 kW. The other two pools with different HRRs have a similar variation law. The flame inclination (θ) is defined as the angle of the flame deviating from the vertical direction. It is evident that the flame inclination increases with increasing rainfall intensity. The impact of raindrop size on the flame inclination is relatively obvious when the rainfall intensity is less than 40 mm/h, and the flame inclination decreases with the increase of raindrop size. The impact of raindrop size on flame inclination decreases gradually with increasing rainfall intensity.

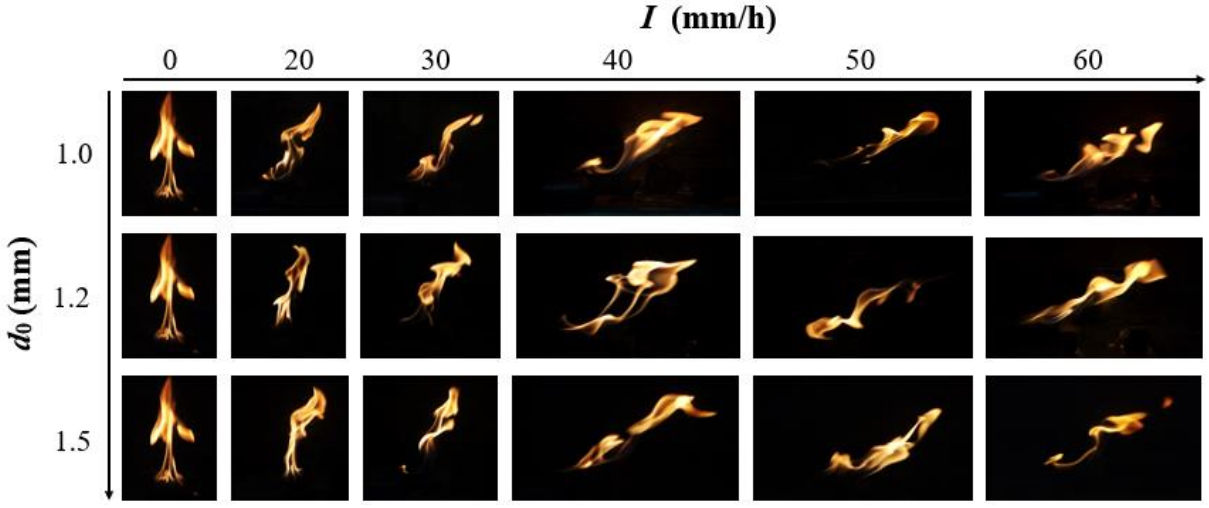

Fig. 4 Flame shape under different I and d_0 with HRR=2.1 kW.

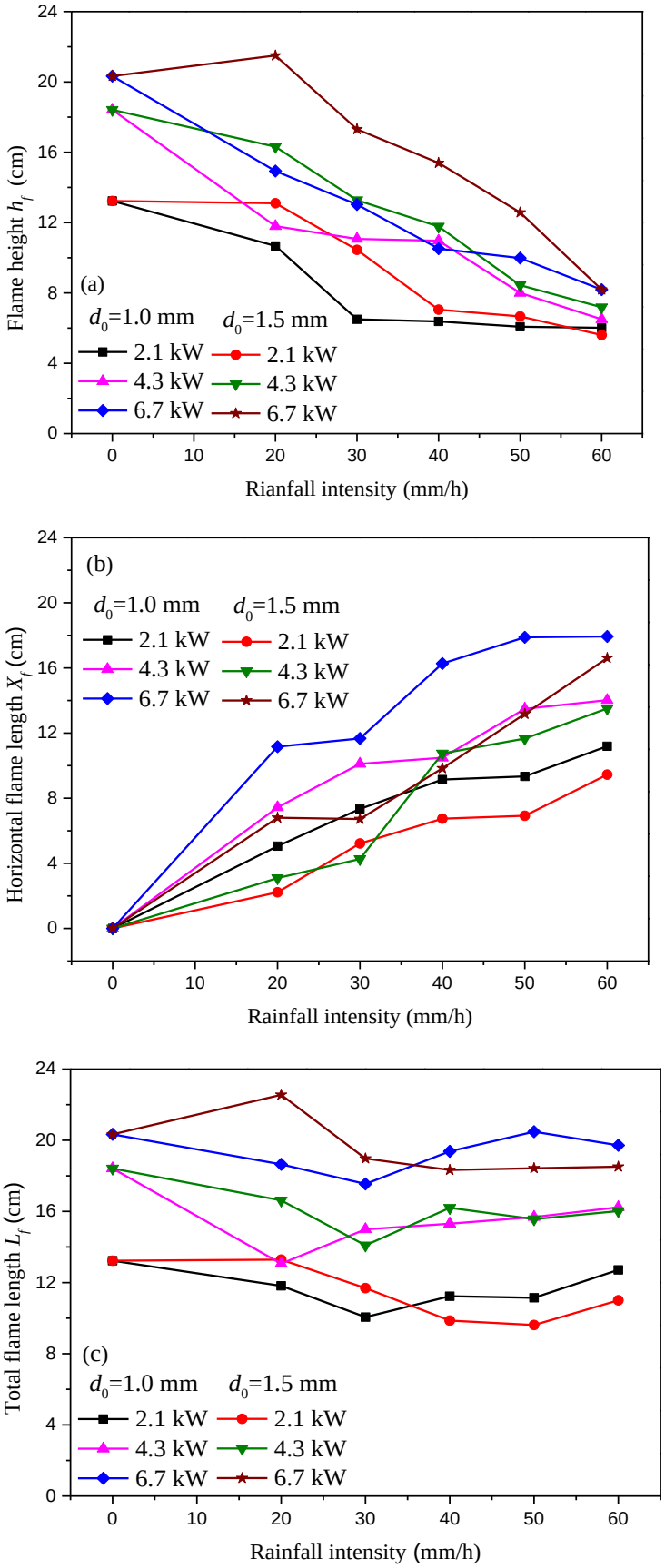

Fig. 5 Variation law of flame shape parameters under different I and d_0.

Figure 5 shows the variation law of flame shape parameters under different rainfall intensities and raindrop sizes. Previous research confirms that a probability of 0.5 for the appearance of flames at each pixel can be used to determine the flame shape [40]. Flame height (h_f) is defined as the vertical distance from the flame tip to the fuel pool surface. Total flame length (L_f) is defined as the linear distance from the fuel pool center to the flame tip, and the horizontal flame length (X_f) is defined as the horizontal projection length of the flame. It is found that the flame height first decreases significantly and then decreases slowly with increasing rainfall intensity for a relatively small pool with HRR=2.1 kW, while the flame height always decreases with the increase of rainfall intensity for the relatively large pools with HRR=4.3 kW and HRR=6.7 kW. Moreover, with increasing rainfall intensity, the horizontal flame length kept increasing and the total flame length first decreases and then increases for all pools with different HRRs.

A dimensionless rainfall intensity I^* was defined as Eq. (8), and the dimensionless Froude number was defined as Eq. (9),

$$I^* = I/(g\dot{m}''d_f/\rho_a)^{1/3} \tag{8}$$

$$Fr = v_{a,0}{}^2/gd_f \tag{9}$$

Dimensionless flame length and flame inclination are related to Froude number and dimensionless rainfall intensity, as shown in Fig. 6. The prediction expressions of flame length and flame inclination are achieved, as shown in Eqs. (10), (11), and (12), respectively.

$$h_f/d_f = 0.89\exp(-1.4I^*\Pi Fr) + 0.74 \tag{10}$$

$$X_f/d_f = (I^*\Pi Fr)^{0.27} \tag{11}$$

$$\tan(\theta) = 0.88(I^*\Pi Fr)^{0.31} \tag{12}$$

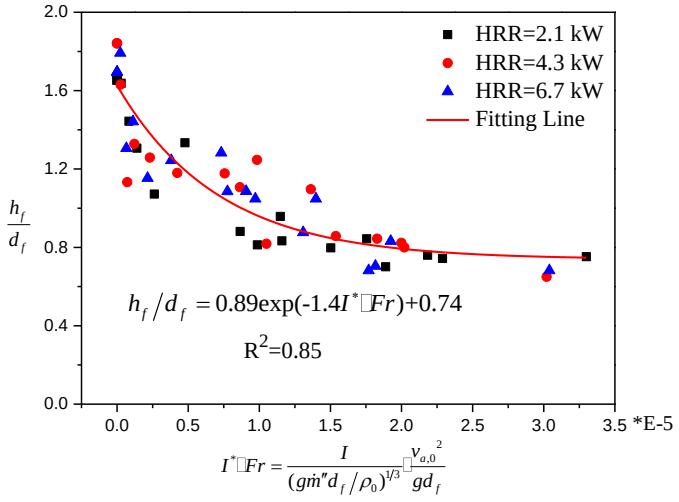

(a) Relationship between h_f/d_f and $I^*\Pi Fr$

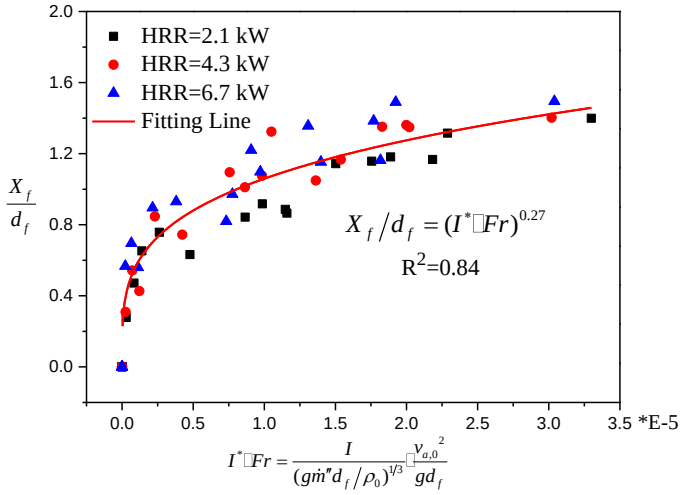

(b) Relationship between X_f/d_f and I^*Fr

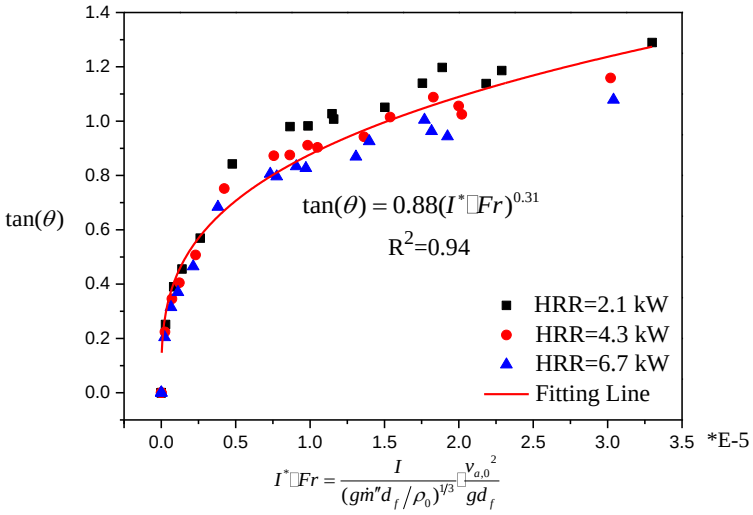

(c) Relationship between $\tan(\theta)$ and I^*Fr

Fig. 6 Relationship among the dimensionless flame length and flame inclination, *Fr* and *I**.

Figure 7 shows the variation of burning rate and heat release rate with rainfall intensity and raindrop size. It can be found that compared with the flame shape, the burning rate of the hydrocarbon pool fire occurring inside the tunnels is less affected by the rainfall. The reason is the fact that the velocity of the longitudinal airflow induced by rainfall is limited. The airflow velocity in the tunnel does not exceed 1 m/s measured in our tests that even when the rainfall intensity reaches 60 mm/h. Previous studies found that ventilation with an airflow velocity of less than 1 m/s has a limited effect on the burning rate of pool fires [41]. However, the burning rate of the pool with different HRRs varies with the rainfall intensity, which is caused by the change in the dominant thermal feedback.

The combustion of fuel is sustained by three major heat feedback sources, namely

conductive heat feedback, convective heat feedback, and radiative heat feedback. All three mechanisms are influential on burning in many practical situations [42]. The velocity of induced airflow increases with the increase of rainfall intensity, resulting in an increase in the flame inclination (as shown in Fig. 4). For the relatively small pool (HRR=2.1 kW), the conductive heat feedback and the convective heat feedback are the dominant mechanisms. Although the radiative heat feedback decreases as the flame inclination increases, heat is transferred from the fuel to the pool rim through the deflected flame, heating the leeward side of the pool. The convective heat feedback also increases under the effect of longitudinal airflow. Therefore, the burning rate of pools increases slightly with increasing rainfall intensity. For the relatively large pools (HRR=4.3 kW and HRR=6.7 kW), the radiative heat feedback is the dominant mechanism. As the rainfall intensity increases to 40 mm/h, the flame inclination increases to about 43°, and the decrease of the view angle leads to the reduction of radiative heat feedback from the flame. Even though there is an increase in convective and conductive heat feedback, its value is smaller than the reduction of radiant thermal feedback. Therefore, a reduction in the burning rate occurs when the rainfall intensity increases to 40 mm/h.

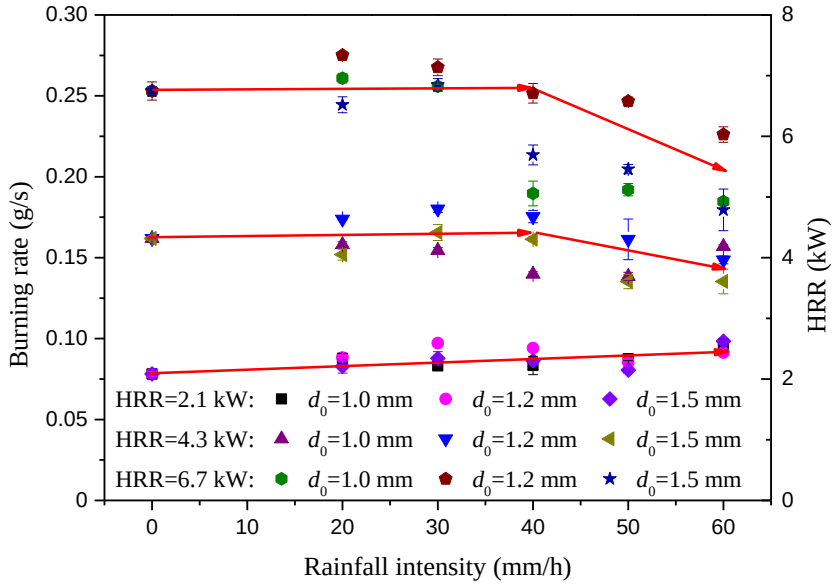

Fig. 7 Variation of burning rate and HRR with I and d_0.

3.3 Ceiling smoke excess temperature

Ceiling temperature distribution plays a crucial role in determining tunnel fire risk [43]. Many studies have investigated the ceiling temperature distribution and reported an exponential attenuation correlation along its longitudinal direction [44]. Figure 8 shows the variation of ceiling excess temperature (ΔT) under rainfall intensity and raindrop size with HRR=2.1 kW and HRR=6.7 kW. It can be clearly observed that the ceiling excess temperature on both sides

of the fire source is symmetrical in the absence of rainfall.

Under rainfall conditions, the point of maximum excess temperature gradually shifts towards the no-rainfall portal, and a higher rainfall intensity results in a decrease in the maximum excess temperature. Moreover, the ceiling excess temperature distribution on both sides of the fire source is less symmetrical because of the competition between the inertial force of the longitudinal airflow induced by rainfall and the thermal driving force of the hot smoke on the rainfall side. With the increase in rainfall intensity, the phenomenon of smoke back-layering occurs gradually.

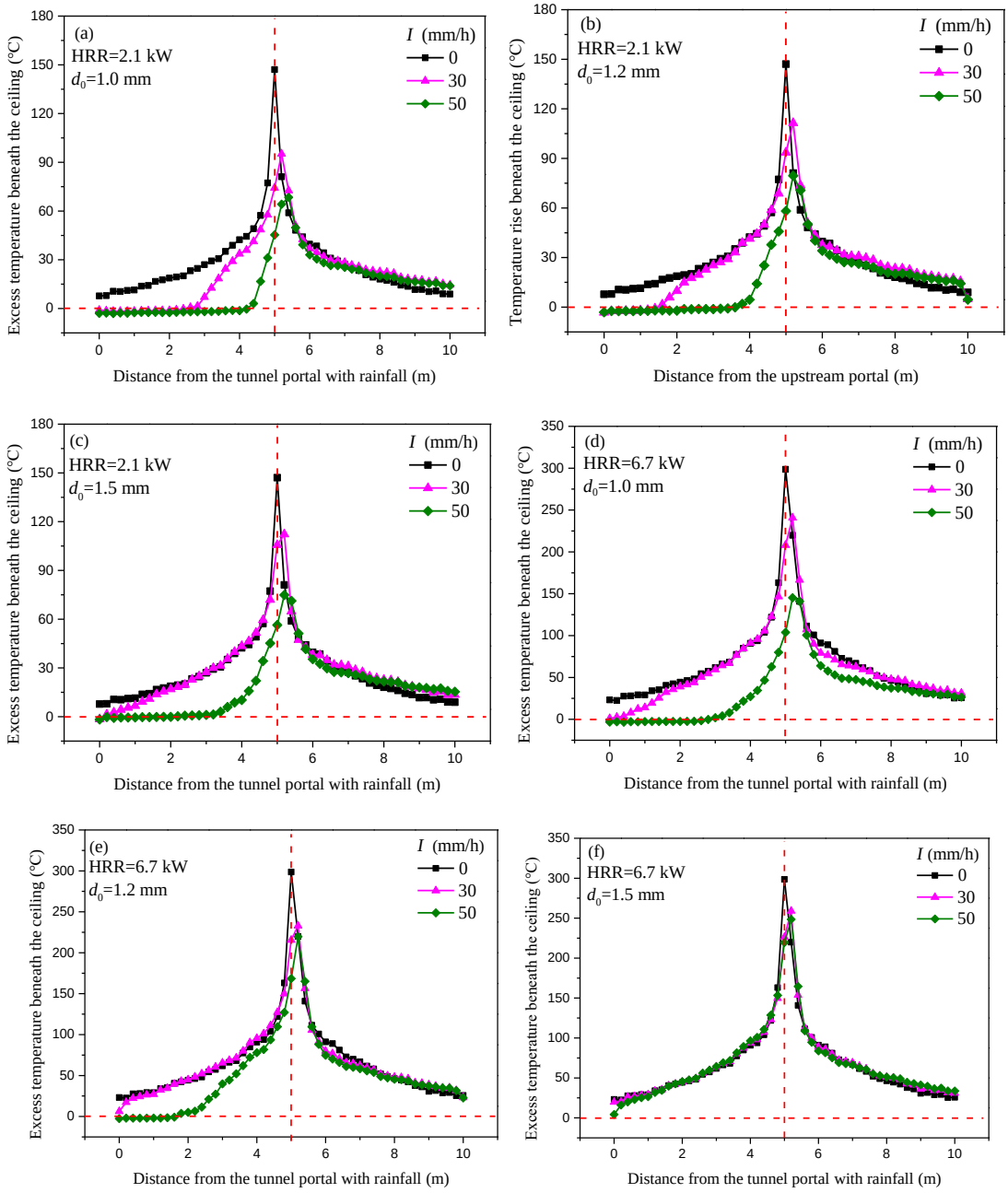

Fig. 8 Variation of ceiling excess temperature under different I and d_0 with HRR=2.1 kW and 6.7 kW.

Compared with the burning rate and flame shape, the movement of hot smoke on the rainfall side is very sensitive to raindrop size. Table 6 shows the smoke back-layering length of the three fire sizes with different rainfall intensities and raindrop sizes. The smoke back-layering length decreases with the increasing rainfall intensity. Under the same rainfall intensity, the smaller raindrop size leads to a decrease in back-layering length. Taking the pool fire with HRR=2.1 kW as an example, the smoke cannot escape from the tunnel portal with rainfall when d_0=1.0 mm and I=20 mm/h, and the smoke back-layering length is 2.0 m when I=30 mm/h. The smoke can escape from the tunnel portal with rainfall when d_0=1.2 mm and I=20 mm/h, and the smoke back-layering length is 3.2 m when I=30 mm/h. It is still not enough to prevent the escape of the smoke when d_0=1.5 mm and I=30 mm/h. The reason is that the rainfall curtain can shield and even prevent the smoke from overflowing towards the portal with rainfall, and smaller raindrops provide a better shielding effect on the smoke [45]. In addition, the buoyancy of hot smoke increases with the HRR, and so does the rainfall intensity required to prevent the smoke from escaping.

Table 6 Smoke back-laying length under different I and d_0.

HRR (kW)	2.1			4.3			6.7		
I (mm/h)	d_0 (mm)								
	1.0	1.2	1.5	1.0	1.2	1.5	1.0	1.2	1.5
0	5.0	5.0	5.0	5.0	5.0	5.0	5.0	5.0	5.0
20	2.8	5.0	5.0	2.8	5.0	5.0	5.0	5.0	5.0
30	2.0	3.2	5.0	2.6	5.0	5.0	5.0	5.0	5.0
40	1.0	1.2	3.0	1.4	3.2	5.0	2.6	3.8	5.0
50	0.4	0.8	1.4	0.8	2.2	2.6	2.0	2.4	5.0
60	0	0.4	0.2	0.4	0.8	2.4	0.4	2.0	2.8

Taking the maximum excess temperature location as the reference for ceiling temperature distribution, Figure 9 shows the attenuation trend of dimensionless excess temperature towards the no-rainfall portal. It can be observed that the ceiling excess temperature distribution can be predicted by Eq. (13), which describes the results well. It indicates that the ceiling excess temperature distribution towards the no-rainfall portal is insensitive to rainfall, which is independent of rainfall intensity and raindrop size.

$$\Delta T/\Delta T_{max} = 0.4\exp[-0.09(x-x_{max})/H]+0.6\exp[-1.36(x-x_{max})/H)] \qquad (13)$$

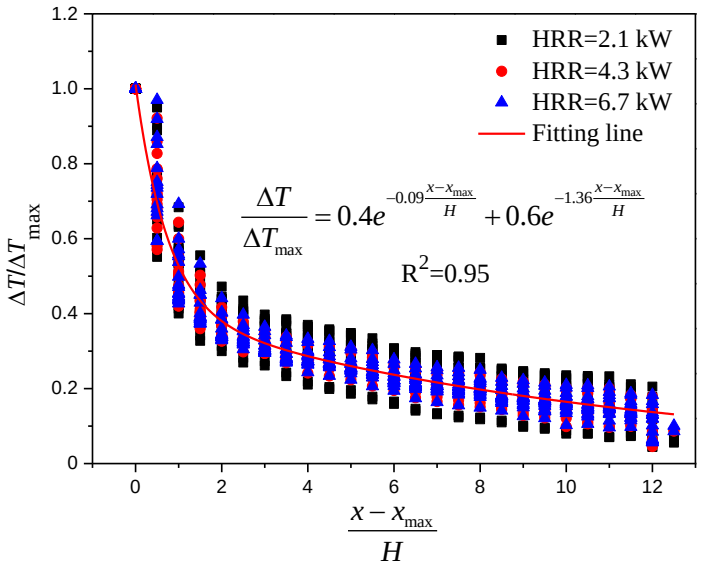

Fig. 9. Attenuation trend of ceiling excess temperature towards the no-rainfall portal.

4. Conclusion

In this paper, model tests were conducted to examine the burning and smoke spreading characteristics of tunnel fires under the action of heavy rainfall on one exit. Following are the main conclusions:

(1) The heavy rainfall can induce a longitudinal airflow inside the tunnel. Such a flow at the portal follows the correlation of $v_{a,0} = I^{\frac{1}{2}} d_0^{-\frac{1}{4}}$, so it increases with the rainfall intensity while decreasing as the raindrop diameter increases.

(2) The rainfall-induced airflow tilts the flame towards the no-rainfall portal, so the flame height decreases with increasing rainfall intensity. With the increase in rainfall intensity, the horizontal flame length always increases, and the total flame length decreases initially and then increases. Models are developed to predict the flame length and flame inclination of hydrocarbon pool fires in tunnels with rainfall.

(3) The burning rates of pools with different HRRs show different variation laws with rainfall intensity. For the relatively small pool fire (HRR=2.1 kW), the burning rate increases slightly with increasing rainfall intensity. For the relatively large pool fires (HRR=4.3 kW and HRR=6.7 kW), a reduction in the burning rate occurs when the rainfall intensity increases to 40 mm/h (equivalent to 155 mm/h in nature).

(4) Under rainfall, the maximum ceiling excess temperature decreases with the rainfall intensity, and the ceiling temperature distribution on both sides is less symmetrical from the fire source. The raindrop size dramatically impacts the movement of hot smoke on the

rainfall side, while the ceiling temperature distribution towards the no rainfall portal is insensitive to rainfall. A prediction model of ceiling excess temperature distribution towards the no-rainfall portal independent of rainfall intensity and raindrop particle size is proposed.

Acknowledgments

This work was supported by National Natural Science Foundation of China (Grant No. 52278545), and Central South University Research Programme of Advanced Interdisciplinary Studies (Grant No. 2023QYJC024).

References

[1] W. Bank, Turn Down the Heat: Climate Extremes, Regional Impacts, and the Case for Resilience, The World Bank, (2013).
[2] M. Almazroui, F. Saeed, S. Saeed, M. Ismail, M.A. Ehsan, M.N. Islam, M.A. Abid, E. O'Brien, S. Kamil, I.U. Rashid, I. Nadeem, Projected changes in climate extremes using CMIP6 simulations over SREX regions, Earth Syst Environ. 5 (2021) 481-497.
[3] X.L. Liao, W. Xu, J.L. Zhang, Y. Qiao, C.N. Meng, Analysis of affected population vulnerability to rainstorms and its induced floods at county level: A case study of Zhejiang Province, China, Int. J. Disaster Risk Reduc. 75 (2022) 102976.
[4] X.J. Sun, X.M. Shan, H.Q. Xu, J. Wang, Assessment of climate change impacts and urban flood management schemes in central Shanghai, Int. J. Disaster Risk Reduc. 65 (2021) 102563.
[5] Z.L. Ma, C.F. Shao, S.R. Zhang, Characteristics of traffic accidents in Chinese freeway tunnels, Tunn. Undergr. Space Technol. 24 (2009) 350-355.
[6] G. Theofilatos, G. Yannis, A review of the effect of traffic and weather characteristics on road safety, Accid. Anal. Prev. 72 (2014) 244-256.
[7] National Disaster Reduction Center of China (NDRCC), The emergency management department issued the national top ten natural disasters in 2021, (Accessed 23 Feb 2022. Chinese), <http://www.ndrcc.org.cn/zqtj/25732.jhtml>.
[8] A. Haghighat, K. Luxbacher, Determination of critical parameters in the analysis of road tunnel fires, Int. J. Min. Sci. Technol. 29 (2019) 178-198.
[9] M.S. Tomar, S. Khurana, Impact of passive fire protection on heat release rates in road tunnel fire: A review, Tunn. Undergr. Space Technol. 85 (2019) 149-159.
[10] M. Wang, H.N. Liu, F. Wang, L.H. Shen, M.C. Weng, Effect of the metro train on the smoke back-layering length under different tunnel cross-sections, Appl. Sci. 12 (2022) 6775.
[11] T.H. Zhang, G.Y. Wang, J.D. Li, Y.D. Huang, K. Zhu, K. Wu, Experimental study of back-layering length and critical velocity in longitudinally ventilated tunnel fire with various rectangular cross-sections, Fire Saf. J. 126 (2021) 103483.
[12] J. Ji, H.X. Wan, K.Y. Li, J.Y. Han, J.H. Sun, A numerical study on upstream maximum temperature in inclined urban road tunnel fires, Int. J. Heat Mass Transf. 88 (2015) 516-526.
[13] S. Shafee, A. Yozgatligil, An analysis of tunnel fire characteristics under the effects of vehicular blockage and tunnel inclination, Tunn. Undergr. Space Technol. 79 (2018) 274-285.
[14] T. Ishikawa, K. Keita, F. Tanaka, K.A.M. Moinuddin, Combustion efficiency during fires in tunnels

with natural ventilation by vitiated air including descending smoke, Fire Saf. J. 120 (2021) 103093.

[15] Y.B. Huang, Y.F. Li, J.X. Li, K. Wu, H.H. Li, K. Zhu, J.M. Li, Experimental investigation of the thermal back-layering length in a branched tunnel fire under longitudinal ventilation, Int. J. Therm. Sci. 173 (2022) 107415.

[16] Y. Jia, X.L. Fan, X.J. Zhao, X.L. Zhu, W.F. Zhao, Study on the longitudinal ceiling temperature distribution induced by double pool fires in a tunnel, Int. J. Therm. Sci. 168 (2021) 107059.

[17] S. Gannouni, Critical velocity for preventing thermal backlayering flow in tunnel fire using longitudinal ventilation system: Effect of floor-fire separation distance, Int. J. Therm. Sci. 171 (2022) 107192.

[18] C.G. Fan, J. Ji, Y.Z. Li, H. Ingason, J.H. Sun, Experimental study of sidewall effect on flame characteristics of heptane pool fires with different aspect ratios and orientations in a channel, Proc. Combust. Inst. 36 (2017) 3121-3129.

[19] F. Tang, L.H. Hu, L.Z. Yang, Z.W. Qiu, X.C. Zhang, Longitudinal distributions of CO concentration and temperature in buoyant tunnel fire smoke flow in a reduced pressure atmosphere with lower air entrainment at high altitude, Int. J. Heat Mass Transf. 75 (2014) 130-134.

[20] Z.G. Yan, Q.H. Guo, H.H. Zhu, Full-scale experiments on fire characteristics of road tunnel at high altitude, Tunn. Undergr. Space Technol. 66 (2017) 134-146.

[21] F. Wu, R. Zhou, G.S. Shen, J.C. Jiang, K.Y. Li, Effects of ambient pressure on smoke back-layering in subway tunnel fires, Tunn. Undergr. Space Technol. 79 (2018) 134-142.

[22] Y.Z. Yao, Y.Z. Li, H. Ingason, X.D. Cheng, The characteristics of under-ventilated pool fires in both model and medium-scale tunnels, Tunn. Undergr. Space Technol. 87 (2019) 27-40.

[23] P. Lin, C. Zuo, Y.Y. Xiong, K.H. Wang, J.K. Shi, Z.N. Chen, X.X. Lu, An experimental study of the self-extinction mechanism of fire in tunnels, Tunn. Undergr. Space Technol. 109 (2021) 103780.

[24] P. Salizzoni, M. Creyssels, L. Jiang, A. Mos, R. Mehaddi, O. Vauquelin, Influence of source conditions and heat losses on the upwind back-layering flow in a longitudinally ventilated tunnel, Int. J. Heat Mass Transf. 117 (2018) 143-153.

[25] W. Zhong, J.J. Lv, Z.Z. Li, T.S. Liang, A study of bifurcation flow of fire smoke in tunnel with longitudinal ventilation, Int. J. Heat Mass Transf. 67 (2013) 829-835.

[26] F. Tanaka, K. Yoshida, K. Ueda, J. Ji, A simple model for predicting the smoke spread length during a fire in a shallow urban road tunnel with roof openings under natural ventilation, Fire Saf. J. 120 (2021) 103106.

[27] L. Yi, D. Luan, L.L. Yang, T. Chen, H.W. Tao, Z.S. Xu, C.G. Fan, Flow field and fire characteristics inside a tunnel under the influence of canyon cross wind, Tunn. Undergr. Space Technol.105 (2020) 103575.

[28] D. Luan, R.W. Bu, Z.Q. Sheng, C.G. Fan, X.Y. Huang, Experimental study on the impact of asymmetric heavy rainfall on the smoke spread and stratification dynamics in tunnel fires, Tunn. Undergr. Space Technol. 134 (2023) 104992.

[29] China Meteorological Administration, Grade of rainfall process, (Accessed 18 Sep 2019. Chinese), <http://zwgk.cma.gov.cn/zfxxgk/gknr/flfgbz/bz/202102/t20210210_22720363.html>.

[30] Y.J. Huang, Y.P. Wang, L.L. Xue, X.L. Wei, L.N. Zhang, H.Y. Li, Comparison of three microphysics parameterization schemes in the WRF model for an extreme rainfall event in the coastal metropolitan City of Guangzhou, China, Atmos. Res. 240 (2020) 104939.

[31] M.A. Serio, F.G. Carollo, V. Ferro, Raindrop size distribution and terminal velocity for rainfall erosivity studies. A review, J. Hydrol. 576 (2019) 210-228.

[32] R. Lai, X.T. Liu, S. Hu, H. Xiao, F. Xia, L. Feng, H. Li, Raindrop size distribution characteristic differences during the dry and wet seasons in South China, Atmos. Res. 266 (2022) 947.

[33] H.Z. Yu, Froude-modeling-based general scaling relationships for fire suppression by water sprays, Fire Saf. J. 47 (2012) 1-7.

[34] H. Byun, I. Bae, T. Yoon, I. Yang, S. Lee, C.D. Carter, H. Do, Velocity measurements in a supersonic wind tunnel with a novel calibration-free seedless velocimetry utilizing laser-induced shockwaves and a double-line probe system, Int. J. Heat Mass Transf. 184 (2022) 122246.

[35] X.Y. Huang, Critical drip size and blue flame shedding of dripping ignition in fire, Sci. Rep. 8 (2018) 16528.

[36] B.J.M. Crowell, Light and Matter, Chapter 4.3 Newton's Second Law, 2004.

[37] R.G. Salvagin, M.L.S. Indrusiak, F.R. Centeno, Biodiesel oil pool fire under air crossflow conditions: Burning rate, flame geometric parameters and temperatures, Int. J. Heat Mass Transf. 149 (2020) 119164.

[38] S. Suzuki, S.L. Manzello, Investigating effect of wind speeds on structural firebrand generation in laboratory scale experiments, Int. J. Heat Mass Transf. 130 (2019) 135-140.

[39] Q. Chen, T.B.Y. Chen, A.C.Y. Yuen, C. Wang, Q.N. Chan, G.H. Yeoh, Investigation of door width towards flame tilting behaviours and combustion species in compartment fire scenarios using large eddy simulation, Int. J. Heat Mass Transf. 150 (2020) 119373.

[40] Z.H. Zhou, Y. Wei, H.H. Li, R. Yuen, W. Jian, Experimental analysis of low air pressure influences on fire plumes, Int. J. Heat Mass Transf. 70 (2014) 578-585.

[41] L.H. Hu, C. Kuang, X.P. Zhong, R. Fei, X.L. Zhang, D. Hang, An experimental study on burning rate and flame tilt of optical-thin heptane pool fires in cross flows, Proc. Combust. Inst. 36 (2017) 3089-3096.

[42] C.H. Miller, W. Tang, E. Sluder, M.A. Finney, S.S. McAllister, J.M. Forthofer, M.J. Gollner, Boundary layer instabilities in mixed convection and diffusion flames with an unheated starting length, Int. J. Heat Mass Transf. 118 (2018) 1243-1256.

[43] L. Deng, F. Tang, P. Hu, Physical modeling and machine learning of ceiling maximum temperature rise induced by tandem heat sources with unequal heat release rates in a natural ventilation tunnel, Int. J. Heat Mass Transf. 197 (2022) 123333.

[44] H. Ingason, Y.Z. Li, Model scale tunnel fire tests with longitudinal ventilation, Fire Saf. J. 45 (2010) 371-384.

[45] L. Dombrovsky, S. Dembele, J.X. Wen, A simplified model for the shielding of fire thermal radiation by water mists, Int. J. Heat Mass Transf. 96 (2016) 199-209.